ISSN 1027-5495. Functional Materials, 28, No.3 (2021), p. 437-443.
doi:https://doi.org/10.15407/fm28.03.437

Magnetic, structural and photocatalytic properties of spinel ferrite composition $MeFe_2O_4$ (Me = Ni, Mn, Zn) prepared by modified coprecipitation method

***L.A.Frolova*[1], *O.V.Khmelenko*[2]**

[1]Ukrainian State University of Chemical Technology,
8 Gagarina Ave., 49005 Dnipro, Ukraine
[2]Oles Honchar Dnipro National University,
72 Gagarina Ave., 49010 Dnipro, Ukraine

Received August 22, 2020

Composite ferrites $MeFe_2O_4$ (Me = Ni, Mn, Zn) were synthesized by a modified coprecipitation method. To characterize the obtained samples, the methods of X-ray diffraction analysis and vibration magnetometry were used. The dependences of the parameters of the EPR spectra, diffuse reflection spectra, and UV spectra on the composition were also interpreted. It was found that the obtained ferrite nanoparticles have a spinel structure. The lattice parameter decreases with increasing nickel content. The minimum values correspond to the double compositions of Mn–Ni ferrites. The synthesized nanoferrites have a band gap of 1.55 to 2.2 eV. Magnetic properties such as saturation magnetization and coercive force vary greatly depending on the concentration of Mn cations. The photocatalytic activity of the compounds was studied in the decomposition reaction of methylene blue, which was used as a model organic pollutant. It was found that the photocatalytic activity of $ZnFe_2O_4$ and $MnFe_2O_4$ significantly increases with an increase in the content of nickel cations.

Keywords: spinel, diffuse reflection spectra, photocatalytic activity, EPR spectra.

Магнітні, структурні і фотокаталітичні властивості шпінельних феритів $MeFe_2O_4$ (Me = Ni, Mn, Zn), отриманих модифікованим методом співосадження. *Л.А.Фролова, О.В.Хмеленко*

Синтезовано композиційні ферити $MeFe_2O_4$ (Me = Ni, Mn, Zn) модифікованим методом співосадження. Для характеристики отриманих зразків використано рентгенофазовий аналіз, вібраційну магнітометрію. Інтерпретовано залежності параметрів ЕПР спектрів, спектрів дифузного відбиття, УФ спектрів від складу. Встановлено, що отримані наночастинки феритів мають шпінельну структуру. Параметр решітки зменшується зі збільшенням вмісту нікелю. Мінімальні значення відповідають подвійним складам Mn–Ni феритів. Синтезовані наноферити мають енергію забороненої зони між 1,55 і 2,2 еВ. Магнітні властивості, такі як намагніченість насичення та коерцитивна сила, значно змінюються в залежності від концентрації катіонів Mn. Фотокаталітичну активність сполук вивчали в реакції розкладання метиленового синього, який використовували як модельний органічний забруднювач. Встановлено, що зі збільшенням вмісту катіонів нікелю значно збільшується фотокаталітична активність $ZnFe_2O_4$ та $MnFe_2O_4$.

Модифицированным методом соосаждения синтезированы композиционные ферриты $MeFe_2O_4$ (Me = Ni, Mn, Zn). Для характеристики полученных образцов использованы рентгенофазовый анализ, вибрационная магнитометрия. Интерпретированы зависимости параметров ЭПР спектров, спектров диффузного отражения, УФ спектров от состава.

Установлено, что полученные наночастицы ферритов имеют шпинельную структуру. Параметр решетки уменьшается с увеличением содержания никеля. Минимальные значения соответствуют двойным составам Mn–Ni ферритов. Синтезированные нанофериты имеют энергию запрещенной зоны между 1,55 и 2,2 эВ. Магнитные свойства, такие как намагниченность насыщения и коэрцитивная сила, значительно изменяются в зависимости от концентрации катионов Mn. Фотокаталитическую активность соединений изучали в реакции разложения метиленового синего, который использовали как модельный органический загрязнитель. Установлено, что с увеличением содержания катионов никеля значительно увеличивается фотокаталитическая активность $ZnFe_2O_4$ и $MnFe_2O_4$.

1. Introduction

In recent decades, nanodispersed spinel ferrites with the general formula $MeFe_2O_4$ (where Me is a divalent transition metal ion) have attracted the attention of researchers through their various fields of application [1–3].

Numerous studies of structural, optical, electrical and magnetic properties of spinel ferrites have been performed [4–6]. It is obvious that the properties of $MeFe_2O_4$ ferrites (where Me = Mn, Co, Ni, Zn) are significantly influenced by both the chosen synthesis technology and its parameters [7–9]. Technologies for obtaining dispersed spinel ferrites such as hydrothermal method, sonochemical method, sol-gel method, coprecipitation method have been developed [10–17]. Among them, the coprecipitation method is particularly promising due to the short duration of the process, low energy consumption, high purity of the final product, high phase homogeneity of the product and relatively low reaction temperature. The essence of the method is the coprecipitation of iron (III) and Me (II) hydroxides by adding alkalis to solutions of the corresponding salts. Thus, the composition of nanoferrites synthesized by the chemical method of coprecipitation depends on the type of salt used, the ratio of cations, and the initial pH [18–20].

In the spinel structure, the Me^{2+} and Fe^{3+} cations occupy tetrahedral and octahedral positions, respectively. There are three main types of spinel structures: normal, inverted and mixed, depending on the filling of tetrahedral and octahedral sites of the sublattice with divalent and trivalent cations [21]. In normal spinel, divalent and trivalent cations occupy the tetrahedral and octahedral positions, respectively. In mixed spinel, the tetrahedral and octahedral positions are randomly filled with divalent and trivalent cations. In the inverse spinel, tetrahedral sites are completely occupied by trivalent cations and octahedral sites are evenly occupied by divalent and trivalent cations. The very arrangement of cations on the sublattices determines the magnetic properties of the final product.

Spinel structures containing several cations have been insufficiently studied. It is the synthesis of composite ferrites that leads to the improvement of their physical properties. For example, nickel ferrite is a well-known material with moderate coercivity and high saturation magnetization. Manganese ferrite has low coercivity, moderate saturation magnetization in combination with good chemical resistance, high mechanical hardness [11]. These properties, along with their great physical and chemical resistance, determine their widespread use. The distribution of Ni^{2+}, Mn^{2+} and Zn^{2+} cations at tetrahedral and octahedral sites has a significant effect on magnetic and optical parameters [22].

The aim of this work is to obtain ferrites with compositions in the system $MeFe_2O_4$ (Me = Ni, Mn, Zn) by the action of contact nonequilibrium low-temperature plasma; to determine optimal compositions of ferrites using the simplex method. The magnetic and photocatalytic properties were chosen as a criterion of optimality of the obtained samples in the decomposition reaction of methylene blue.

2. Experimental

The preparation of co-precipitated compounds was carried out by pouring with continuous stirring the corresponding mixture of sulphate solutions with the required ratio of cations, as in ferrite. Iron (II) sulphate, nickel sulphate, manganese sulphate, zinc sulphate, sodium hydroxide of analytical purity were used. Subsequent processing was carried out by CNP for 30 min.

The processing was carried out in a cylindrical reactor with an inner diameter of 45 mm and a height of 85 mm. Cooling of the reaction mixture was provided by continuous circulation of cold water in the outer jacket. The electrodes were made of stainless steel, one of which (4 mm in diameter) was located in the lower part of the reactor, and the other (2.4 mm in diameter)

Table 1. Simplex lattice planning matrix {3, 3}

No.	Formula	Ni	Mn	Zn	y
1	$NiFe_2O_4$	1.00	0	0	y_1
2	$Ni_{0.67}Mn_{0.33}Fe_2O_4$	0.667	0.33	0	y_{122}
3	$Ni_{0.33}Mn_{0.67}Fe_2O_4$	0.333	0.667	0	y_{112}
4	$MnFe_2O_4$	0	1.00	0	y_2
5	$Mn_{0.67}Zn_{0.33}Fe_2O_4$	0	0.667	0.33	y_{223}
6	$Mn_{0.33}Zn_{0.67}Fe_2O_4$	0	0.333	0.667	y_{233}
7	$ZnFe_2O_4$	0	0	1.00	y_3
8	$Ni_{0.33}Zn_{0.67}Fe_2O_4$	0.33	0	0.667	y_{133}
9	$Ni_{0.67}Zn_{0.33}Fe_2O_4$	0.667	0	0.333	y_{113}
10	$Ni_{0.33}Zn_{0.33}Mn_{0.33}Fe_2O_4$	0.333	0.333	0.333	y_{123}

was placed above the solution surface at a distance of 10 mm. To obtain a plasma discharge, a voltage of 500 was applied to the electrodes. A vacuum pump was used to reduce the pressure in the reactor. The plasma method in more detail is described in [23–25].

X-ray diffraction patterns of the samples were obtained on a DRON-2.0 instrument with monochromatic $CoK\alpha$ radiation. The size of the crystallites was determined using the Scherer formula.

Magnetic characteristics were determined using a vibrating magnetometer. Electronic paramagnetic resonance (EPR) spectra were obtained using a Radiopan SE/X-2543 radio spectrometer. Intensity and width of the signal, and resonant frequency were used to characterize the EPR signals.

UV-VS spectroscopy was used to analyze the optical properties of powdered ferrites. The results were used to calculate the energy of the band gap. The band gap energy was determined from the diffuse reflection spectra of the samples using the Kubelka-Munch function.

Catalytic decomposition experiments were performed in a glass vessel at 25°C with continuous shaking. As a radiation source, an UV lamp DKB 9 was used with an effective spectral range of 180–275 nm. The intensity of ultraviolet radiation was about 3 mW/cm^2. The lamp was placed above the solution at a distance of 10 cm from its surface. Before adding the catalyst, the maximum absorption of the model solution was measured using a spectrophotometer in the range of 200–900 nm. Changes in the initial optical density were monitored by taking an aliquot of the solution at regular intervals and subjecting it to spectroscopic analysis. The concentration of methylene blue (MB) was determined spectrophotometrically using a UV 5800 PC spectrometer.

The degree of decomposition was calculated from the decrease in the concentration of MB in aqueous solution by the formula:

$$\%X = \frac{(C_0 - C_t) \cdot 100\%}{C_0}, \quad (1)$$

where C_0 is the initial concentration of MB in solution, mol/l; C_t is the concentration of MB in solution at time t, mol/l.

To study the influence of the cationic composition on the properties of ferrites, a simplex lattice plan was used, which requires a minimum number of experiments to study the influence of factors on the selected response functions. The molar concentrations of nickel, manganese and zinc, respectively, were chosen as factors x_1, x_2, x_3. The plan of the experiment is shown in Table 1.

The calculation of the coefficients in the regression equation and verification of its adequacy was performed using the program STATISTICA 12. Diagrams of "properties-composition" were plotted using isolines. The response functions were coercive force (H_c), Oe; saturation magnetization (Ms), Emu/g; a is the lattice parameter, Å; X_{MB} is the degree of decomposition of methylene blue, %; E is the energy of the band gap, eV.

3. Results and discussion

3.1 Characteristics of ferrite samples

Fig. 1 shows X-ray diffraction patterns of nickel ferrite, manganese ferrite and zinc ferrite. The patterns have indexed peaks (111), (220), (311), (222), (400), (422), (511) and (440). The indexed peaks corre-

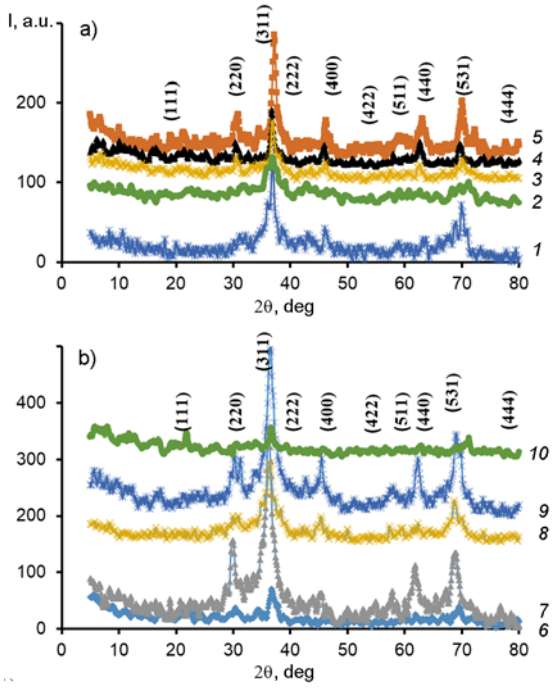

Fig. 1. XRD pattern of ferrites: a) — samples 1, 2, 3, 4, 5, b) — samples 6, 7, 8, 9, 10.

spond to a typical spinel phase, which is in good agreement with the JCPDS charts 22-1086, 10-0325, 88-1965. The diffraction patterns show a decrease in intensity and expansion of the peaks with increasing manganese concentration in both the Ni–Mn and Zn–Mn ferrite systems (samples 1–4, 4–7).

Weak diffuse scattering at small angles indicates the presence of a small amount of substance in the amorphous state along with crystalline phases in the investigated materials. The X-ray diffraction pattern also shows broad peaks indicating the nanodispersed nature and small size of crystallites in the samples. In addition, weak peaks on

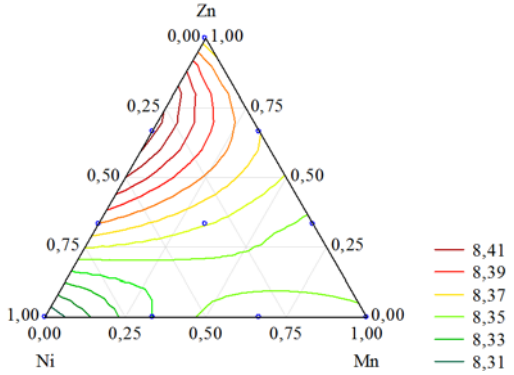

Fig. 2. Dependences of the lattice parameter on the composition of ferrites.

the diffraction patterns of sample 7 indicate the presence of a small amount of hematite α–Fe_2O_3 in the sample under study.

Diffraction patterns of nickel, manganese and zinc ferrites can be interpreted as a result of superposition of reflections from powder particles with an average particle size of 200–400 Å.

The lattice parameter decreases as the nickel concentration increases. The minimum values correspond to the double compositions of Mn–Ni. A more pronounced increase in the lattice parameter is observed for samples 1–4, a small increase for 4–7 and a decrease for 8–10. This indicates the replacement of the smaller Ni^{2+} ion (0.69 Å) by the larger Mn^{2+} ion (0.80 Å) and, accordingly, Mn^{2+} (0.80 Å) by Zn^{2+} (0.74 Å) (Fig. 2, Table 2). The most important are the magnetic characteristics of the material, which are determined by recording the magnetization curves at room temperature. Various parameters, such as saturation magnetization (M_s) and coercive force (H_c), are derived from the magnetization curves

Table 2. The results of the experiment

N	Ni	Mn	Zn	H_c, Oe	M_s	Emu/g	H_R	mT	I_R	abs.unit
1	1	0	0	2	26.05	364	2429	8.3209	96.44	1.92
2	0.667	0.333	0	8	7.35	340	2282	8.3408	76.13	1.7
3	0.333	0.667	0	38	41.69	358	2327	8.3583	95.04	1.8
4	0	1	0	41	111	352	2322	8.3592	44.58	1.55
5	0	0.667	0.333	8	47.7	307	2851	8,343	81.75	1.71
6	0	0.333	0.667	8	3.75	343	2439	8.366	88	9
7	0	1	19	3.93	342	3008	8.3689	24.43	2.2	
8	0.333	0	0.667	9	7.7	345	3692	8.4231	95.31	1.88
9	0.667	0	0.333	7	19	359	3824	8.3795	74.47	1.82
10	0.3333	0.3333	0.3333	44	37.8	407	2103	8.36025	81.81	1.7

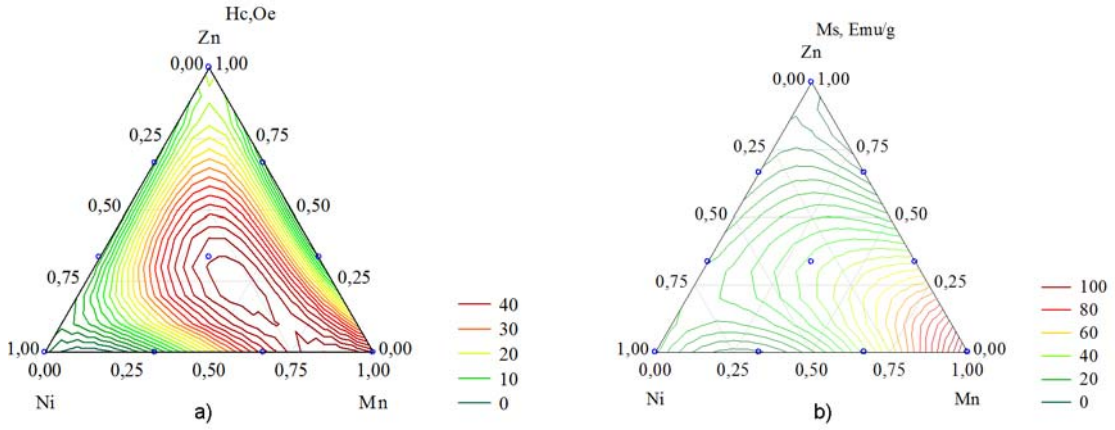

Fig. 3. Dependences of coercive force (a) and saturation magnetization (b) on the composition of samples (Table 1).

shown in Table 2. Figure 3 shows that the coercive force for all samples is small. In addition, the saturation magnetization of $MnFe_2O_4$ is much higher than in other samples (M_s is 111.8 Emu/g for $MnFe_2O_4$).

Diffuse reflection spectra were obtained to evaluate the optical properties of ferrites. All 10 samples showed an intense absorption band in the UV region of the electromagnetic spectrum. The band gap in the samples was determined by the equation

$$\alpha h\nu = A(h\nu - E)^n,\ n = 2, \qquad (2)$$

where α is the absorption coefficient, ν is the frequency of light, E is the energy of the band gap, eV, and A is the proportionality constant.

The band gaps calculated for $NiFe_2O_4$, $MnFe_2O_4$, $ZnFe_2O_4$ were 1.92 eV, 1.59 eV, 2.2 eV, respectively, and were slightly lower than those reported in [26, 27].

The energy of the ferrite band gap is shown in Table 2. It increases with increasing Zn content (Fig. 4a). Significant variations in the energy of the band gap can be observed due to the difference in the average crystallite size, lattice constant, phase purity, concentration of the charge carriers and deformation of the crystal lattice.

Comparison of the dependences of the band gap on the composition and the intensities of the peaks in the EPR spectra makes it possible to determine the most significant of the listed factors (Fig. 4b).

The results of processing the EPR spectra of photocatalysts are shown in Fig. 4b. Two indicators were chosen as the evaluation criterion: the intensity of the peak of the EPR spectrum and the value of the resonant frequency. Zn^{2+} ions with a fully filled d orbital do not contribute to the EPR signal in the case of an excited state. The dependence of the peak intensity on the number of electrons in the last orbital can be clearly seen. For nickel, the number of d electrons is 8, for zinc — 10, for manganese — 5.

Studies of the photocatalytic activity of ferrites showed that the degree of decomposition of MB in the presence of ferrite photocatalysts was 90–96 % within 60 min after UV exposure. Fig. 4 shows that the photocatalytic activity of ferrites increases with an increase in the number of Ni ions. MB degradation increases from 44 % for $MnFe_2O_4$ to 96 % for $Ni_{0.33}Mn_{0.66}Fe_2O_4$ and $Ni_{0.33}Zn_{0.66}Fe_2O_4$ after 60 minutes of UV light irradiation.

The results of the reactivity of individual ferrites are much lower than the double and triple compositions (Table 2).

4. Conclusions

For use as photocatalysts, ferrites MFe_2O_4 (M = Ni, Mn, Zn) were synthesized by a combined method of coprecipitation and subsequent plasma treatment.

The regularities of the change in the properties of ferrites were studied by the method of simplex lattice planning of the experiment. The obtained dispersed ferrites were characterized by X-ray phase analysis, EPR spectroscopy, UV spectroscopy, vibration magnetometry. The role of cations in the decomposition of methylene blue has been established. The most effective catalysts were ferrites containing nickel. Synthesized samples containing nickel and manganese have high magnetic properties; they are easily separated from the aqueous solution under the influence of an external

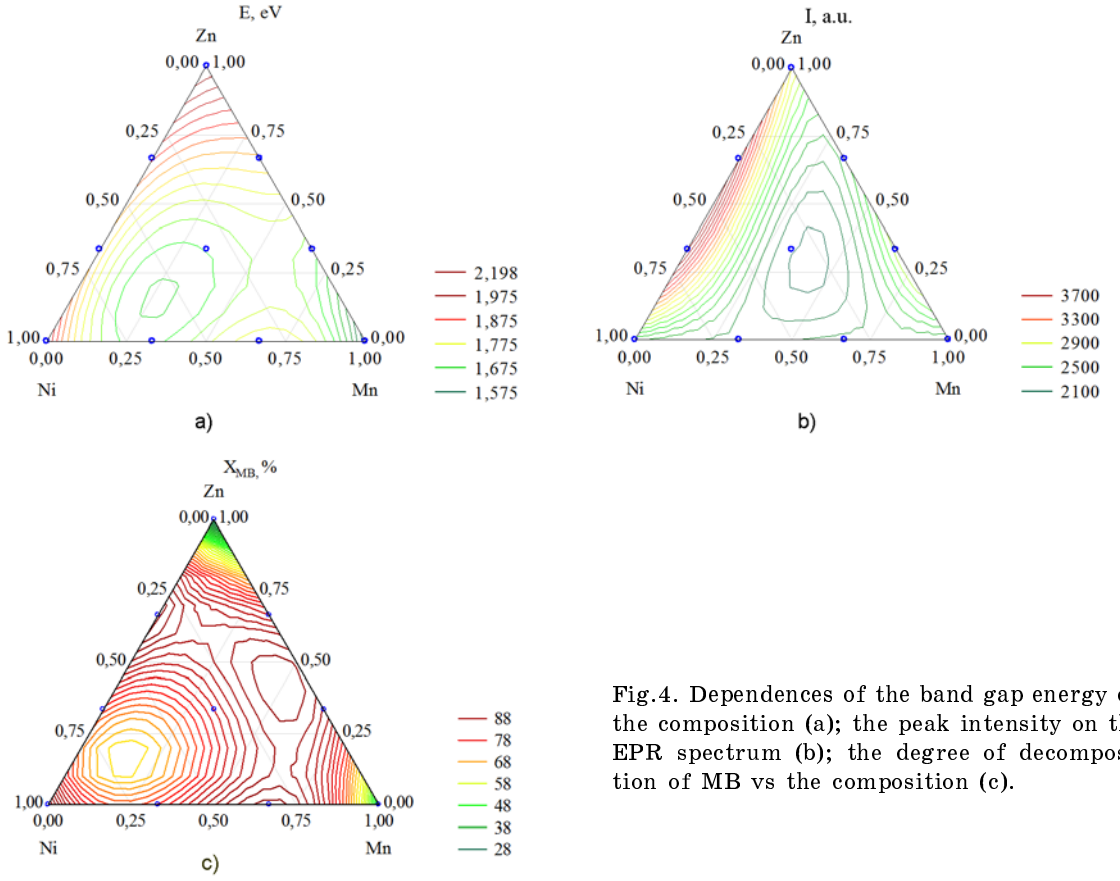

Fig.4. Dependences of the band gap energy on the composition (a); the peak intensity on the EPR spectrum (b); the degree of decomposition of MB vs the composition (c).

magnetic field. The intensity of the peaks in the EPR spectrum and the gap energy in the range correlate with each other. The degree of MB degradation is inversely proportional to the energy of the band gap.

References

1. R.Sharma, P.Thakur, M.Kumar et al., *J. Alloy. Compd.*, **746**, 532 (2018).
2. F.Vetr, Z.Moradi-Shoeili, S.Ozkar, *Appl. Organomet. Chem.*, **32**, e4465 (2018).
3. K.Bindu, H.S.Nagaraja, *Mater. Res. Express*, **6**, 095015 (2019).
4. A.Pathania, S.Bhardwaj, S.S.Thakur et al., *Physica B: Condensed Matter*, **531**, 45 (2018).
5. M.A.Maksoud, G.S.El-Sayyad, A.Abokhadra et al., *J. Mater. Sci.:Mater. Electron.*, **31**, 2598 (2020).
6. S.O.Aisida, P.A.Akpa, I.Ahmad et al., *Physica B: Condens. Matt.*, **571**, 130 (2019).
7. S.Sanatombi, S.Sumitra, S.Ibetombi, *Iran. J. Sci. Technol. A*, **42**, 2397 (2018).
8. N.I.Abu-Elsaad, S.A.Mazen, H.M.Salem, *J. Alloy. Compd.*, **835**, 155227 (2020). https://doi.org/10.1016/j.jallcom.2020.155227
9. A.K.Tyagi, D.S.Ahlawat, *Orient. J. Chem.*, **33**, 296 (2017).
10. B.I.Kharisov, H.R.Dias, O.V.Kharissova, *Arab. J. Chem.*, **12**, 1234 (2019). DOI: 10.1016/j.arabjc.2014.10.049
11. M.A.Almessiere, Y.Slimani, A.D.Korkmaz et al., *J. Supercond. Nov. Magn.*, **32**, 3837 (2019). DOI: 10.1007/s10948-019-05147-z
12. R.S.Melo, P.Banerjee, A.Franco, *J. Mater. Sci.: Mater. Electron.*, **29**, 14657 (2018). DOI: 10.1007/s10854-018-9602-2
13. K.Jalaiah, K.V.Babu, *J. Magn. Magn. Mater.*, **423**, 275 (2017). DOI: 10.1016/j.jmmm.2016.09.114
14. L.Frolova, A.Pivovarov, E.Tsepich, *J. Chem. Technol. Metall.*, **51**, 163 (2016).
15. P.Dolcet, S.Diodati, F.Zorzi et al., *Green Chem.*, **20**, 2257 (2018). DOI: 10.1039/C8GC00086G
16. F.Ding, J.Lin, T.Wu, H.Zhong, *Appl. Phys. A*, **126**, 1 (2020). DOI: 10.1007/s00339-020-3406-y
17. Y.Liu, J.Hsu, *Appl. Sci.*, **8**, 1005 (2018). DOI: 10.3390/app8061005
18. S.Mirzaee, Y.Azizian-Kalandaragh, P.Rahimzadeh, *Solid State Sci.*, **99**, 106052 (2020). DOI: 10.1016/j.solidstatesciences.2019.106052
19. H.Harzali, A.Marzouki, F.Saida et al., *J. Magn. Magn. Mater.*, **460**, 89 (2018). DOI: 10.1016/j.jmmm.2018.03.062

20. I.Szczygiel, K.Winiarska, A.Sobianowska-Turek, *J.Therm.Anal.Calorim.*, **134**, 51 (2018). DOI: 10.1007/s10973-018-7417-2
21. J.S.Smart, *Am.J.Phys.*, **23**, 356 (1955). DOI: 10.1119/1.1934006
22. F.Ding, J.Lin, T.Wu et al., *Appl.Phys.A* **126**, 221 (2020). DOI: 10.1007/s00339-020-3406-y
23. L.Frolova, A.Pivovarov, E.Tsepich, in: Fesenko O., Yatsenko L. (eds) Nanophysics, Nanophotonics, Surface Studies, and Applications. Springer Proc. Physics, vol. 183, Springer, Cham. DOI: 10.1007/978-3-319-30737-4_18
24. L.A.Frolova, M.P.Derhachov, *Nanoscale Res. Lett.*, **12**, 1 (2017). 505. DOI: 10.1186/s11671-017-2268-5
25. L.Frolova, A.Pivovarov, T.Butyrina, *Pigment & Resin Technology*, **46**, 356 (2017). DOI: 10.1108/PRT-07-2016-0073
26. P.Iranmanesh, S.Saeednia, M.Mehran et al., *J. Magn.Magn.Mater.*, **425**, 31 (2017). DOI: 10.1016/j.jmmm.2016.10.105
27. R.S.Yadav, I.Kuritka, J.Vilcakova et al., *J. Phys.Chem.Solids*, **110**, 87 (2017). DOI: 10.1016/j.jpcs.2017.05.029